Applied Physics B (2021) 127:12
https://doi.org/10.1007/s00340-020-07565-7

Applied Physics B
Lasers and Optics

Design method of variable optical path length multi-pass cell

Zhenxi Zhang[1] · Hongguang Zhou[1] · Xufei Chen[1] · Yunfeng Bi[1]

Received: 4 October 2020 / Accepted: 12 December 2020 / Published online: 10 January 2021

Abstract
According to the basic principle of the Herriott-type multi-pass cell (MPC), this paper analyzes the relationship between the optical path length (OPL) and the distance of the mirrors, and proposes a design method of variable optical path length MPC, which makes it easier to implement variable optical path length MPC. In the design, the incident angle is controlled to arrange the spots in a circle on the concave mirrors, and a method of adjusting the distance between the reflectors and the position of the exit point is proposed to realize the continuous and controllable numbers of passes (integer). MPC is frequently used to improve the sensitivity of gas detection, and the variable OPL designation is helpful for gas detecting of wide concentration range and the exploration of noise compensation methods in MPC.

1 Introduction

MPC can increase the interaction path for the beam and matter by confining the incident beam to reflect back and forth between two or more mirrors, and combining the MPC with TDLAS [1–3], Raman spectroscopy [4, 5], photoacoustic spectroscopy [6, 7] and other technologies which can effectively improve the detection sensitivity [8–10]. The White-type [11] and Herriott-type [12] are the most commonly used MPCs. The former is characterized by a larger aperture angle and can achieve more numbers of passes, but it requires more mirrors and more complex structure [9], and is not easy to adjust. Compared with the White-type MPC, the Herriott-type MPC is simple in structure, small in size, relatively easy to adjust the beam path, and is widely used in systems with the laser source.

For low-concentration gas detection, a long OPL gas cell is usually needed to improve sensitivity; for high-concentration gas, there is no need for a long OPL [13]. To meet the needs of different detection sensitivities and ranges, OPL should be variable in MPC. In trace gas detection applications based on TDLAS technique, the gas detection sensitivity is fundamentally determined by the absorbed intensity and signal–noise ratio [14, 15]. MPC can increase the intensity of the absorption signal by increasing the OPL, which can effectively improve the detection sensitivity, but the multiple passes will cause stronger interference noise [16–20]. There is insufficient research on interference noise in MPC, which hinders performance improvement to a certain extent. MPC with variable OPL is of great value for studying the influence of noise under different OPLs, different numbers of passes, and different beam paths, as well as exploring noise compensation methods.

Currently, the research on MPC focuses on multi-channel [2, 21–23] and long OPL [24–26] detection. Most Herriott-type MPCs on the market have a fixed cavity length, which makes it difficult to adjust the OPL. In the research of variable optical path length MPC, J. Altmann et al. adjusted the number of passes by changing the distance between two parallel concave mirrors to obtain different OPLs [20]. The variable range of the distance of the concave mirror is between *f* and *2f*. However, the adjustable range is small, and the number of passes and OPL are not continuous.

Based on the basic principles [21, 27, 28] proposed by Herriott et al., this paper analyzes the circular arrangement conditions for the reflex spots, the constraints for the spot size, the number of passes and the distance between the mirrors (0 ~ 4f). Combining the geometric transmission characteristics of ray, a design method for MPCs with

✉ Yunfeng Bi
byf@sdu.edu.cn

Zhenxi Zhang
zzx19961223@outlook.com

Hongguang Zhou
1694945345@qq.com

Xufei Chen
1461038291@qq.com

[1] School of Mechanicals, Electrical and Information Engineering, Shandong University, Weihai 264200, China

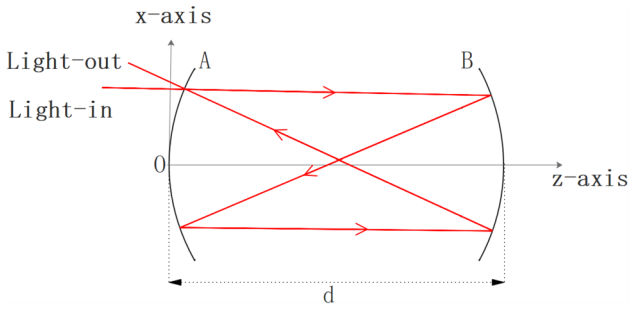

Fig. 1 Schematic diagram of Herriott-type MPC. The beam is reflected back and forth between two identical and coaxial spherical mirrors, *A* and *B*, in the *x*–*z* plane of a Cartesian coordinate system

variable OPL is proposed, which realizes a variable OPL in a wide range with better continuity.

2 Design principle for Herriott absorption cell

The Herriott-type MPC is composed of two parallel concave mirrors, which are placed on the *x*–*y* plane, as shown in Fig. 1.

Generally, the spots on the mirror form an elliptical pattern, and the order of the spots in the pattern or track depends on the distance between the mirrors [12, 18, 21, 27]. In order to make full use of the surface of the concave mirror and to facilitate the setting of the entrance and exit holes, the spots on the concave mirror should be designed in circular arrangement. The distance between the mirrors affects the number of passes and changes the OPL. To meet the required different OPLs, the relationship between the OPL and the mirrors distance must be clarified. To prevent rays from prematurely overflowing from the entrance hole and the mutual interference between adjacent spots during multiple passes, it is necessary to control the actual spot size [29, 30].

2.1 Distribution of spots

Assume that the incident point is (x_0, y_0) and the direction vector of the incident beam is (x_0', y_0', z_0'). In order to simplify the calculation, the direction vector z_0' is normalized to 1. The slope of the incident beam is (x_0', y_0'). After n passes, the intersection of the beam and the spherical mirror is (x_n, y_n), the focal length of the two spherical mirrors is f, and the center distance is d. Basing on Pierce's results[31], Herriott et al. obtained formula (1) [20, 24, 25]:

$$x_n = x_0 \cos n\theta + \sqrt{\frac{d}{4f-d}}\left(x_0 + 2fx_0'\right)\sin n\theta \tag{1}$$

As shown in Fig. 2, the variable θ is the angle between two successive reflections, where the nth point of reflection lies on one mirror and the next point of reflection lies on another. The angle θ depends on the focal length f and the distance d of the spherical mirror, as shown in Eq. (2):

$$\cos\theta = 1 - \frac{d}{2f} \tag{2}$$

When $0 < d < 4f$, the beam can be reflected infinitely between the two mirrors without overflow.

Converting formula (1) into the form of formula (3)

$$x_n = A\sin(n\theta + \alpha) \tag{3}$$

then

$$A^2 = \frac{4f}{4f-d}\left(x_0^2 + dx_0x_0' + dfx_0'^2\right) \tag{4}$$

$$\tan\alpha = \sqrt{\frac{4f}{d} - 1}\left(1 + 2f\frac{x_0'}{x_0}\right) \tag{5}$$

Similarly, the y-direction coordinate y_n of the intersection point of the beam after n passes

$$y_n = B\sin(n\theta + \beta) \tag{6}$$

for formula (6),

$$B^2 = \frac{4f}{4f-d}\left(y_0^2 + dy_0y_0' + dfy_0'^2\right) \tag{7}$$

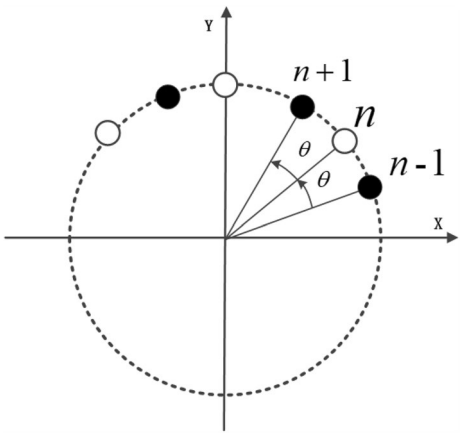

Fig. 2 The spots distribution diagram on reflector *B*. The solid spots represent reflection points on mirror *B*, whereas the circles represent reflection points on the other mirror

$$\tan\beta = \sqrt{\frac{4f}{d} - 1}\left(1 + 2f\frac{y_0'}{y_0}\right) \tag{8}$$

According to formulas (3) to (8), (x_n, y_n) is related to the incident point (x_0, y_0), the incident beam slope (x_0', y_0'), f and d. In general, the spots are distributed in an ellipse, but in special cases, the spots will be distributed in a circle on the spherical mirror, when

$$A = B \tag{9}$$

and

$$\alpha = \beta \pm \frac{\pi}{2} \tag{10}$$

When the following Eqs. (11) and (12) are satisfied, the spots will be arranged in a circle on the spherical mirror

$$\left(x_0^2 - y_0^2\right) + dx_0 \cdot x_0' - dy_0 \cdot y_0' + dfx_0'^2 - dfy_0'^2 = 0 \tag{11}$$

$$\frac{4f^2}{x_0 y_0}x_0' y_0' + \frac{2f}{x_0}x_0' + \frac{2f}{y_0}y_0' + \frac{4f}{d} = 0 \tag{12}$$

where x_0 and y_0 are not *0*.

After the spherical mirrors are selected, the focal length f is determined, and the incident point (x_0, y_0) is fixed, it can be seen from Eqs. (11) and (12) that, when the spots are arranged in a circle on the spherical mirror, the incident angle of the beam is only related to the distance d between two mirrors. For example, the focal length of the spherical mirror is selected as 100 mm, the mirror distance d is set to 170 mm, and incident point of the beam is at (1, 12.4). The incident direction of the beam can be calculated as: $x_0' = 0.06723$, $y_0' = -0.06802$, as shown in Fig. 3. It can be found that the spots show a circle on the spherical mirror.

2.2 Control of spots size

The size of the spots is crucial for the design of the variable optical path length MPC. By calculating the size of the spots and combining the position of the spots, it is possible to monitor the overlap of adjacent spots on the mirrors and the ray leakage during transmission. Figure 4 shows ray leakage and spots overlap respectively. Both of these situations will cause errors in the final detection results. In order to avoid spots interference and ray leakage during the OPL adjustment process, it is necessary to control the spots size.

When the number of passes is 118, the spots overlap each other.

When the beam is continuously reflected between two mirrors, the size of each spot on the mirror will change

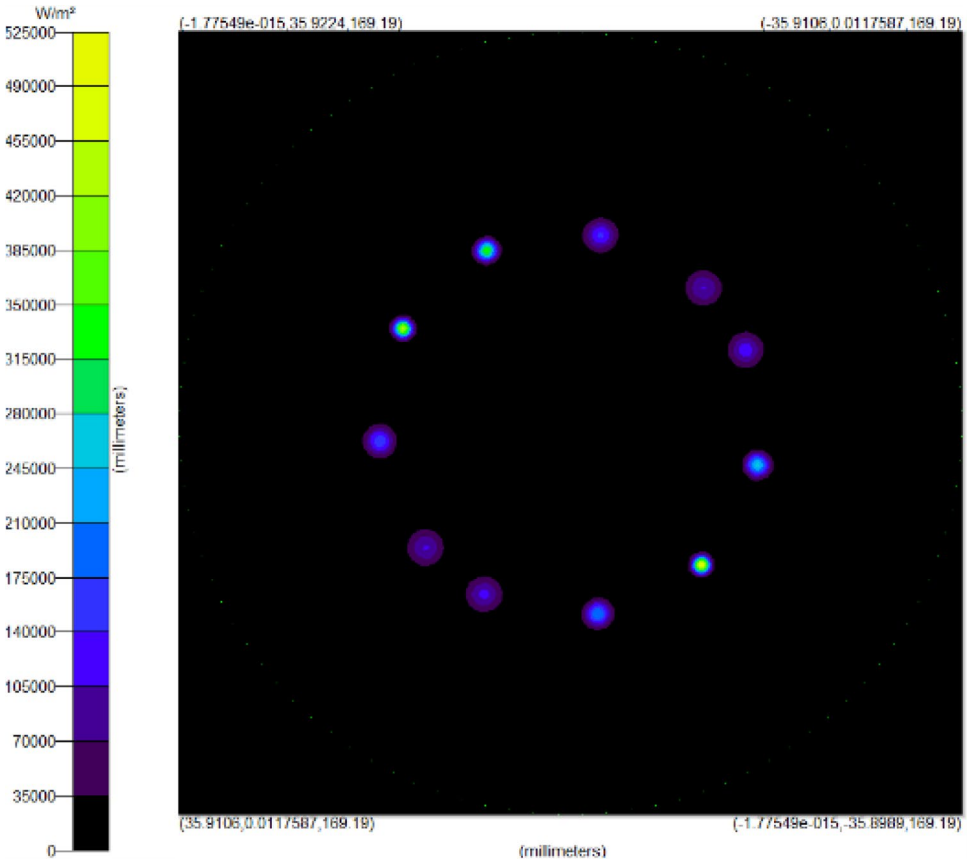

Fig. 3 Spots distribution diagram on spherical mirror *B*

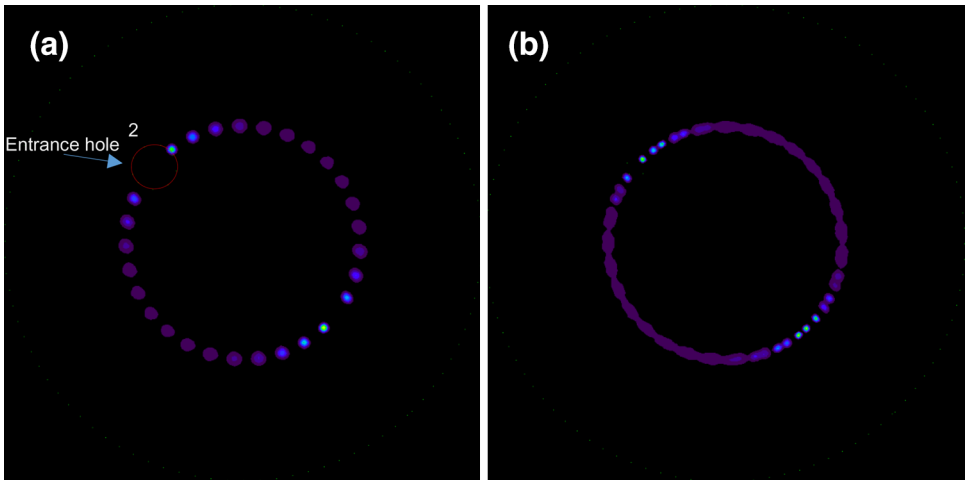

Fig. 4 **a** Spots distribution of mirror *A*. When the number of passes is 58, it can be seen that part of the rays from the second spot leak from the entrance hole **b** Spots distribution on the mirror *A*

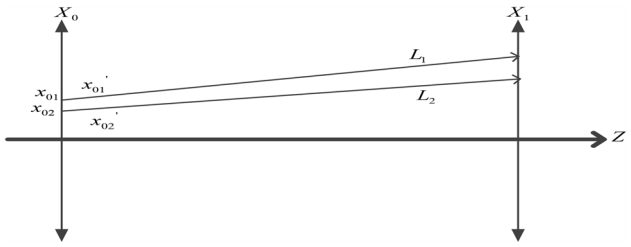

Fig. 5 The profile of the beam on the x–z plane

according to a certain rule. In order to obtain the spot size, it is necessary to track the edge of the beam with a certain divergence angle. As shown in Fig. 5, in the z-axis direction, the contour lines of the incident beam are L_1 and L_2, the incident position coordinates of the two lines in the x-axis direction are x_{01}, x_{02} respectively, and the slopes are $x_{01}^{'}, x_{02}^{'}$ respectively. After n passes, the diameter of the spot is R_L:

$$R_L = |x_{n1} - x_{n2}| = \left|A_1 \sin\left(n\theta + \alpha_1\right) - A_2 \sin\left(n\theta + \alpha_2\right)\right| \tag{13}$$

The y-axis direction is similar to the x-axis direction.

According to formulas (1), (3), (5) and (13), formula (14) can be obtained

$$R_L = \left|\left(x_{01} - x_{02}\right)\cos n\theta + \sqrt{\frac{d}{4f-d}}\left(x_{01} - x_{02} + 2f\left(y'_{01} - x'_{02}\right)\sin n\theta\right)\right| \tag{14}$$

The size of the nth spot is related to the initial beam diameter, the focal length, the distance between the mirrors, the number of passes and the beam divergence angle. Therefore, the size of spot can be controlled by selecting the above parameters. Under the condition of focal length of 100 mm, mirrors spacing of 180 mm, and the initial beam diameter of 1 mm, the size and position distribution of spots on the mirror B are calculated using this model. As shown in Fig. 6a, the spots are equally spaced on the concentric circles of the entrance hole. Setting in TracePro according to the same parameters, performing ray tracing, and analyzing the reflective surface of mirror B, the simulation result is shown in Fig. 6b. It can be seen that the spots distribution pattern obtained by this theory is basically the same as the reflection pattern simulated in TracePro, which can prove the feasibility of the spots size calculation model.

2.3 The number of passes

It can be seen from formula (2) that the included angle θ between two adjacent spots is determined by the distance between the mirrors d and the focal length f of the mirrors. Herriott et al. proposed that if the ray satisfies the following condition

$$n\theta = 2\mu\pi \tag{15}$$

the beam will pass through the incident point again after n passes, that is $(x_0, y_0) = (x_n, y_n)$. μ represents the number of complete turns of the reflection point around the mirror with the angle θ as the step. The number of passes n starts from 0 and increases in steps of 2, and the integer μ increases in steps of 1.

The angle θ is

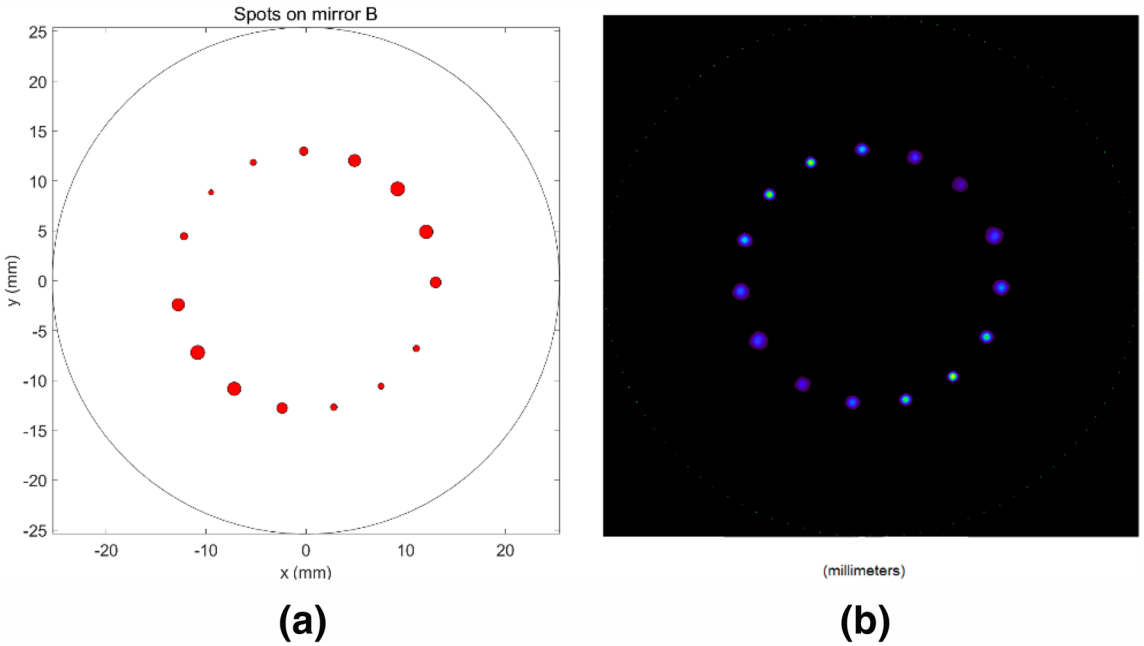

Fig. 6 **a** Theoretical calculation of spots size; **b** Spots distribution in TracePro

$$\theta = \arccos\left(1 - \frac{d}{2f}\right) \tag{16}$$

where $0 < d < 4f$.

There may be multiple sets of solutions satisfying Eqs. (15) and (16) at the same time. However, each one of these solutions differs slightly from each other in the pattern that is produced on the mirror surfaces from the points of reflection [19]. To describe the differing patterns, the variables k and p are introduced. In order to avoid confusion, formula (17) is used to express families of solutions, and a particular solution in a family using the notation n, μ, k, p [21, 27]

$$n = 2p\mu + k \tag{17}$$

where $k = \pm 2, \pm 4, \pm 6\ldots$, p is a positive integer.

From formulas (15) ~ (17), the number of passes n can be expressed as a function of d, k, and p, as shown in Fig. 7.

$$n = \frac{k\pi}{\pi - p \cdot \arccos\left(1 - \frac{d}{R}\right)} \tag{18}$$

Given the radius of curvature and the mirrors spacing, θ is a fixed value according to formula (16). In the families with the same p value, the number of passes n is unique; however, due to the existence of the common factor, there will be multiple numbers of passes and the lower value of n will be obtained. For example, solutions {30, 7, 2, 2}, {60, 14, 4, 2}, {90, 21, 6, 2} and {120, 28, 8, 2} have the same value of θ and d for a given radius of curvature, but the numbers of passes are different. However, the beam will coincide with the spot at $n = 0$ after 30 passes and leave the MPC from the entrance hole. Therefore, only low-order solution of {30, 7, 2, 2} can be obtained. So, μ must be restricted as formula (19) shows

$$(k'\mu) \bmod (k) \neq 0 \tag{19}$$

where $k' < k$, and k' and k are an even [21, 27].

According to the formula (19), when $k = \pm 4, \pm 6, \pm 8, \pm 10$, μ cannot be divisible by 2, 3, 2, and 5 respectively. When $k = \pm 2$, there is no restriction on μ.

In order to obtain better OPL continuity, the numbers of passes (integer) can be continuous by adjusting the position of the exit hole. When the entrance hole is the same as the exit hole, the numbers of passes are not continuous. For example, for the solution family $n = 4\mu - 2$, when the number of turns μ increases in steps of 1, the achievable numbers of passes are shown in Table 1.

However, according to the design method of this paper, the numbers of passes (integer) can be continuous. For the family $n = 4\mu - 2$, when the number of turns μ is incremented by 1, the numbers of passes (even) achieved are not continuous on the even number. u can take values of 1.5, 2.5…, the number of passes will be continuous on even numbers, and an arbitrary number of passes can be realized in the solution family $n = 4\mu - 2$. Since the specific position of each reflection point can be determined, the purpose of

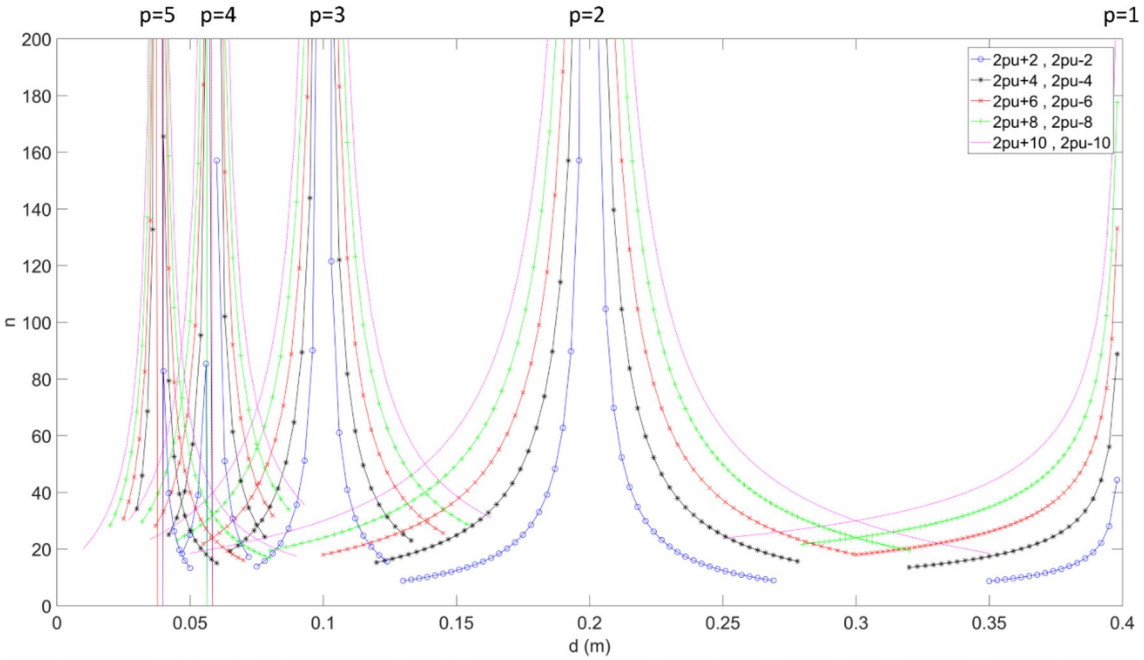

Fig. 7 The relationship between the number of passes n and the distance d of the mirrors when the focal length $f = 100$ mm

Table 1 The value of μ and n, when $n = 4\mu - 2$

μ	1	2	3	4	5	6	7	8	…
n	2	6	10	14	18	22	26	30	…

changing the number of passes can be realized by controlling the position of the exit point. Similarly, for all solutions, $k = \pm 2$ is taken when the value of p is 1, 2, 3, 4… When the position of the exit point is controlled, the beam leaves the MPC at the corresponding number of passes.

The mirrors spacing can be changed continuously, but the number of passes n can only be an integer. For example, the value of d is 170 mm, n is 20.86 in the solution family $n = 4\mu + 2$, but $n = 20$ is obtained by rounding down. When the focal length is fixed, n is only related to d and the number of passes is continuous on $n = 2p\mu \pm 2$ (n is an integer) by controlling the position of the exit point. Therefore, the controllable number of passes can be realized by changing mirrors spacing and adjusting the position of the exit hole.

2.4 Optical path length

1. $d > R$

In order to calculate the OPL, the two spherical mirrors and the beam are geometrically analyzed in a three-dimensional form. In Fig. 8, O' is the perpendicular intersection point of the incident point to the optical axis; r is the distance from the incident point to the optical axis; the surface where O' and the incident point are located in the distribution surface, Q is the curvature center of the spherical mirror B, P is the projection point of the normal on the distribution surface, and d is the vertex spacing of two mirrors. Distance t from the center of curvature Q to the distribution surface of mirror B is

$$t = \sqrt{R^2 - r^2} \tag{20}$$

The angle δ between the normal and the optical axis is

$$\delta = \arctan\left(\frac{r}{t}\right) \tag{21}$$

The distance s from Q to the distribution surface of spherical mirror A is

$$s = d + t - 2R \tag{22}$$

The distance v from the normal projection point to the optical axis is

$$v = s \cdot \tan(\delta) \tag{23}$$

Distance w from point Q to point P is

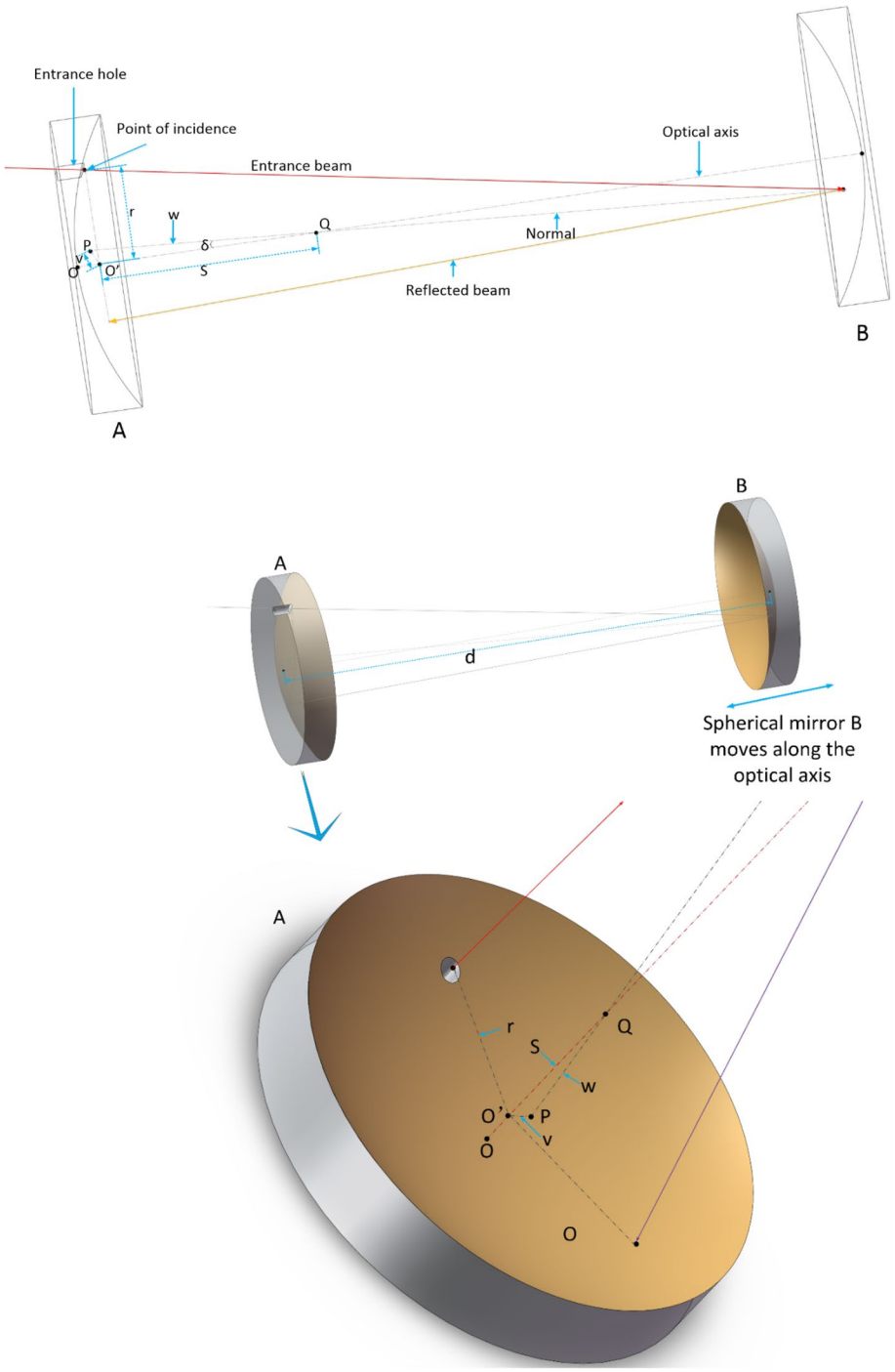

Fig. 8 Geometric analysis of ray and spherical mirror when $d > R$

$$w = \sqrt{s^2 + v^2} \tag{24}$$

When $d > R$, single optical path length OD is

$$\mathrm{OD} = \sqrt{(R + w)^2 + r^2 - v^2} \tag{25}$$

2. $d < R$ (Fig. 9)

Distance t from the center of curvature Q to the distribution surface is

$$t = \sqrt{R^2 - r^2} \tag{26}$$

The angle δ between the normal and the optical axis is

$$\delta = \arctan\left(\frac{r}{t}\right) \tag{27}$$

The distance s from Q to the distribution surface of spherical mirror A is

$$s = 2R - d - t \tag{28}$$

The distance v from the normal projection point to the optical axis is

$$v = s \cdot \tan(\delta) \tag{29}$$

Distance w from point Q to point P is

$$w = \sqrt{s^2 + v^2} \tag{30}$$

When $d < R$ single optical path OD is

$$\mathrm{OD} = \sqrt{(R - w)^2 + r^2 - v^2} \tag{31}$$

When $0 < d < 4f$, according to formulas (20) to (31), the two cases of $d > R$ and $d < R$ are merged into the following formula,

$$\mathrm{OD} = \sqrt{R^2 + r^2 + (d + t - 2R)^2 + 2R(d + t - 2R)\sqrt{1 + \frac{r^2}{R^2 - r^2}}}as \tag{32}$$

Through formula (32), it can be found that OD is a function of d, R, and r. When the spherical mirror is selected and the entrance hole is determined, OD is only related to d. The total path length L after n passes

$$L = n \cdot \mathrm{OD} \tag{33}$$

Since the number of passes n is only related to d when the focal length and reflection mode are fixed, and the optical path length OD of a single pass is only related to d, it can be seen that the L is a function of d.

$$L = \frac{2\pi}{\pi - p \cdot \arccos\left(1 - \frac{\Delta d}{R}\right)}\sqrt{A + (d + B)^2 + 2R(d + B)\sqrt{1 + \frac{r^2}{t^2}}} \tag{34}$$

where $A = \mathrm{R}^2 + \mathrm{r}^2, B = t - 2\,\mathrm{R}$.

From formula (34), the relationship between the OPL and the distance d can be known, and the size of the distance between the mirrors under different OPLs can be obtained, thus the spherical mirror B is moved to the corresponding position. According to formula (18), the number of passes n corresponding to different d can be known. The corresponding number of passes can be achieved by adjusting the position of the exit hole, which fulfills the purpose of obtaining the corresponding OPL.

3 Examples and analysis

3.1 Basic parameters

In order to use the mirror surface more effectively, the position of the entrance hole should be close to the edge of the mirror to make the spots more dispersed. The upper limit of the OPL is related to the power of the incident beam and the mirror reflectivity, which can be increased by selecting a suitable laser and mirror coating. The gold-plated mirror is used, which has reflectivity generally higher than 99%. On the other side, large size hole

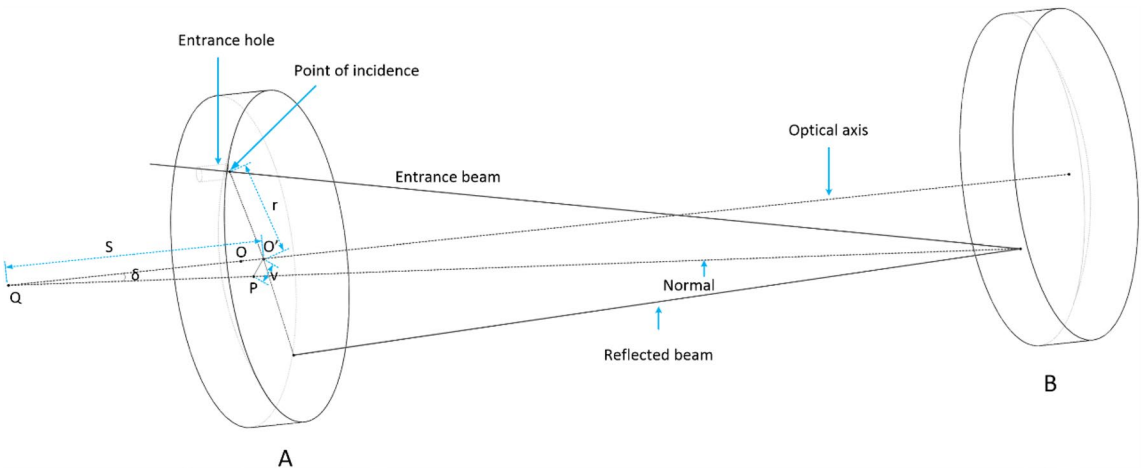

Fig. 9 Geometric analysis of ray and spherical mirror when $d < R$

Table 2 Absorption cell design parameters

Parameter	Value
Specular reflectivity	> 99.2%
Mirror focal length	100 mm
Mirror diameter	25.4 mm
Entrance hole position (mm)	(12,16)
Diameter of entrance hole	1.2 mm

Table 3 Light source parameters

Parameter	Value
Wavelength	5 μm
Light source position (mm)	(12,16,1.38)
Divergence angle	8 mrad
Luminous flux	0.75 W
Beam diameter	1 mm

will cause ray leakage and has an effect on the number of passes. An entrance hole diameter of 1.2 mm is used here. The specific parameters are shown in Table 2.

To avoid the interference of adjacent spots, the light source should be properly selected to make the spot size as small as possible. The light source type is Gaussian light source. The specific parameters are shown in Table 3.

3.2 The distance between spherical mirrors

The required OPL L is 19.8200 m, the relationship diagram between L and the distance d can be obtained, as shown in Fig. 10.

Multiple values of d can satisfy the required OPL. For a smaller d, when more numbers of passes are needed, the spots on the spherical mirror are too dense. Therefore, $d = 193.9$ mm, 206.5 mm and 398.3 mm are selected, and the corresponding numbers of passes are $n = 102$, 96 and 48 respectively, as shown in Fig. 11.

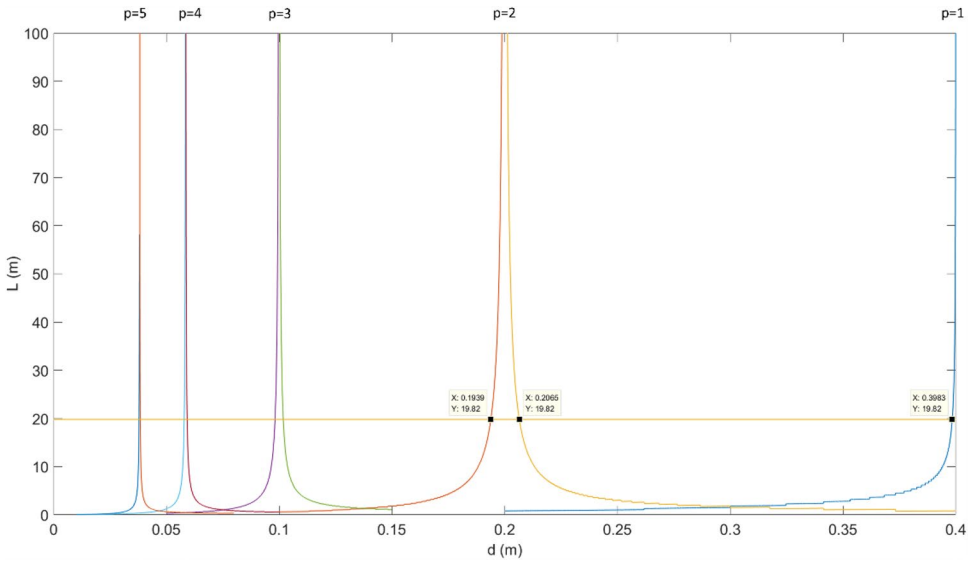

Fig. 10 Diagram of the relationship between L and d

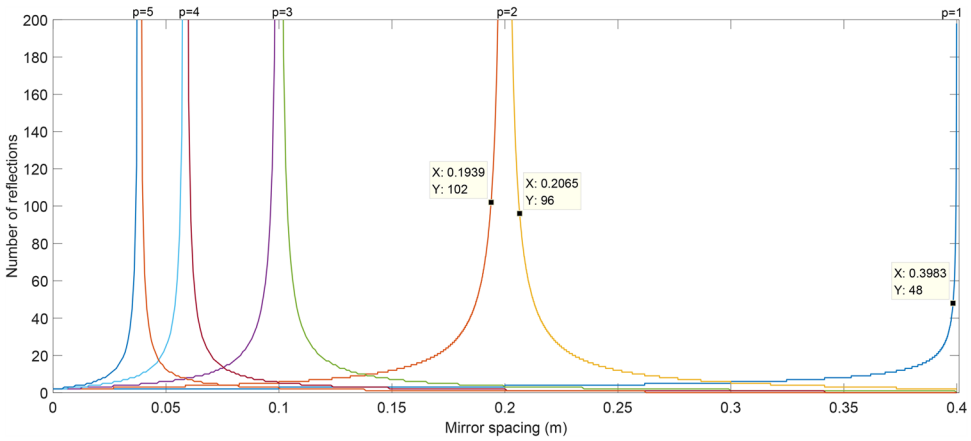

Fig. 11 The relationship between n and d under the corresponding system parameters

Table 4 Spot distribution when $d = 193.9$ mm

Spot number	*X* Pos (mm)	*Y* Pos (mm)	Spot size (mm)
…	…	…	
100	− 3.2677	− 19.8185	1.0402
101	− 19.6168	2.5421	0.9894
102	1.8461	19.9995	0.9789
…	…	…	

Table 5 Spot distribution when $d = 206.5$ mm

Spot number	*X* Pos (mm)	*Y* Pos (mm)	Spot size (mm)
…	…	…	
94	2.0125	19.985	0.9101
95	19.634	− 2.43258	1.0545
96	− 3.09562	− 19.8525	0.9787
…	…	…	

Table 6 Spot distribution when d = 398.3 mm

Spot number	*X* Pos (mm)	*Y* Pos (mm)	Spot size (mm)
…	…	…	
46	− 18.9083	− 7.5454	1.1810
47	− 16.5371	− 11.8018	1.1551
48	14.9421	13.6621	1.1108
…	…	…	

Now, it can be known that the condition for the spots on the spherical mirror to be arranged in a circle is: when $d = 193.9$ mm, 206.5 mm, 398.3 mm, the direction (x_0', y_0') of the incident beam can be obtained as: (0.02251, −0.1419), (0.01744, −0.1381), (−0.05488, −0.08372). And the position of each spot on the spherical mirror and the size of each spot can be obtained in three cases. As shown in Tables 4, 5 and 6 respectively, the even-numbered spots are distributed on spherical mirror *A*, and the odd-numbered spots are on mirror *B*.

According to the specific position and size of the spots, a suitable exit hole can be set to ensure that the number of passes meets the requirements. For example, when $d = 193.9$ mm and the required number of passes is 102, an exit hole with a diameter of 0.98 mm should be set at the point (1.8461, 19.9995) of the spherical mirror *A* placed on the *x*–*y* plane.

3.3 Design results and analysis

By building the Herriott-type MPC model in TracePro and setting the light source according to the semiconductor laser light source, the above design is simulated and verified. In the three cases where *d* is different, the spot distribution diagrams are shown in the Figs. 12, 13, and 14 respectively.

When values of *d* are different, the spots can be arranged in a circle on the reflector by setting the corresponding incident angle. The required number of passes *n* and the OPL can be realized by setting a suitable exit hole

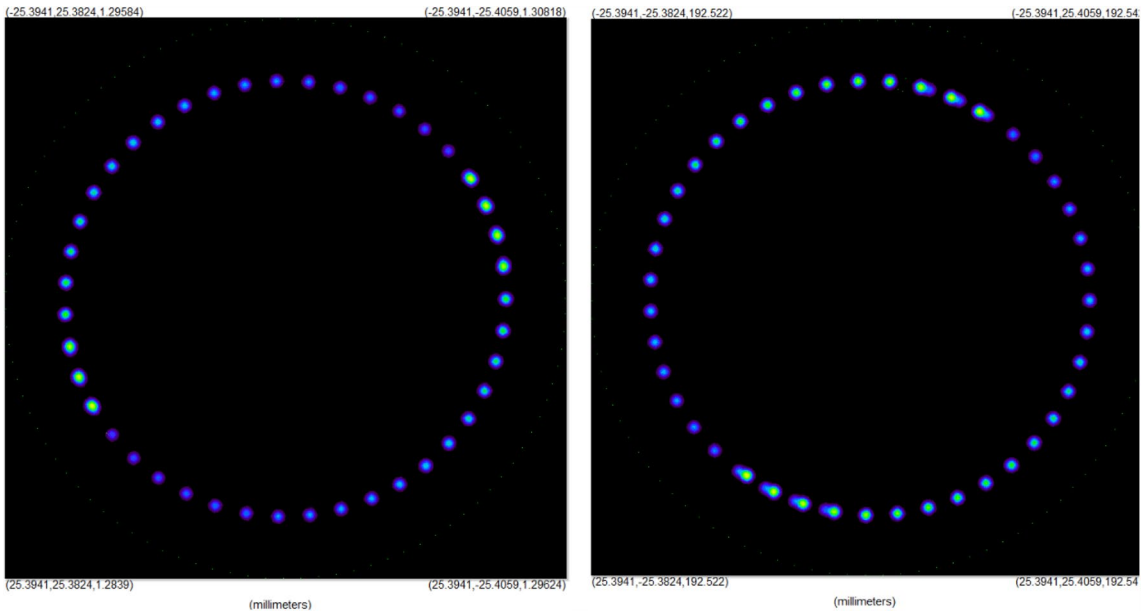

Fig. 12 Spot distribution diagram when $d = 193.9$ mm (the left side is spherical mirror *A*, the right side is spherical mirror *B*)

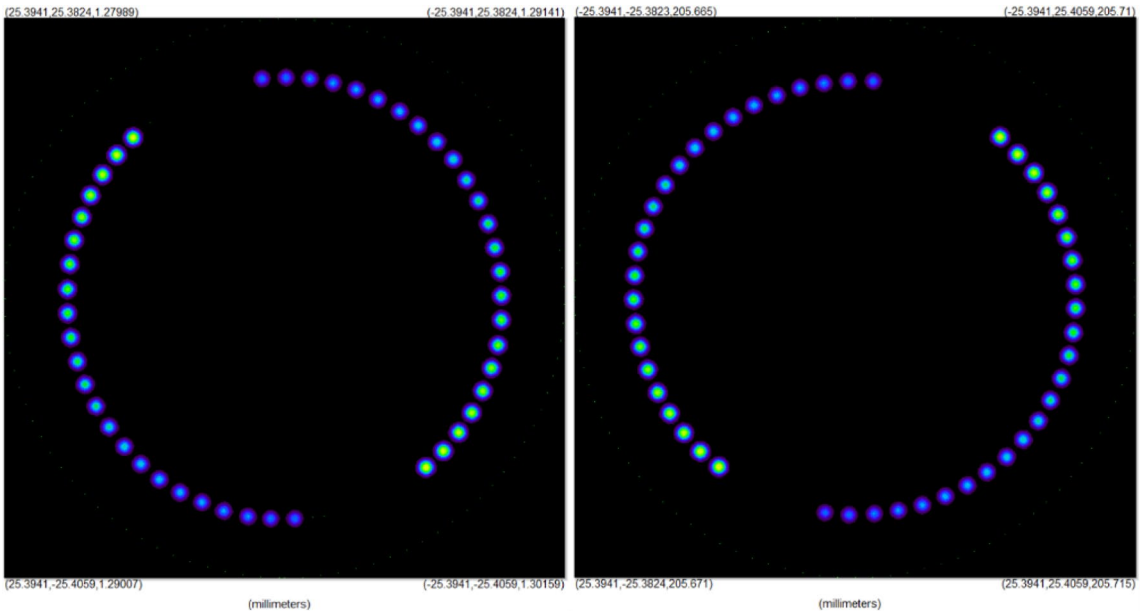

Fig. 13 Spot distribution diagram when $d = 206.5$ mm (the left side is spherical mirror A, the right side is spherical mirror B)

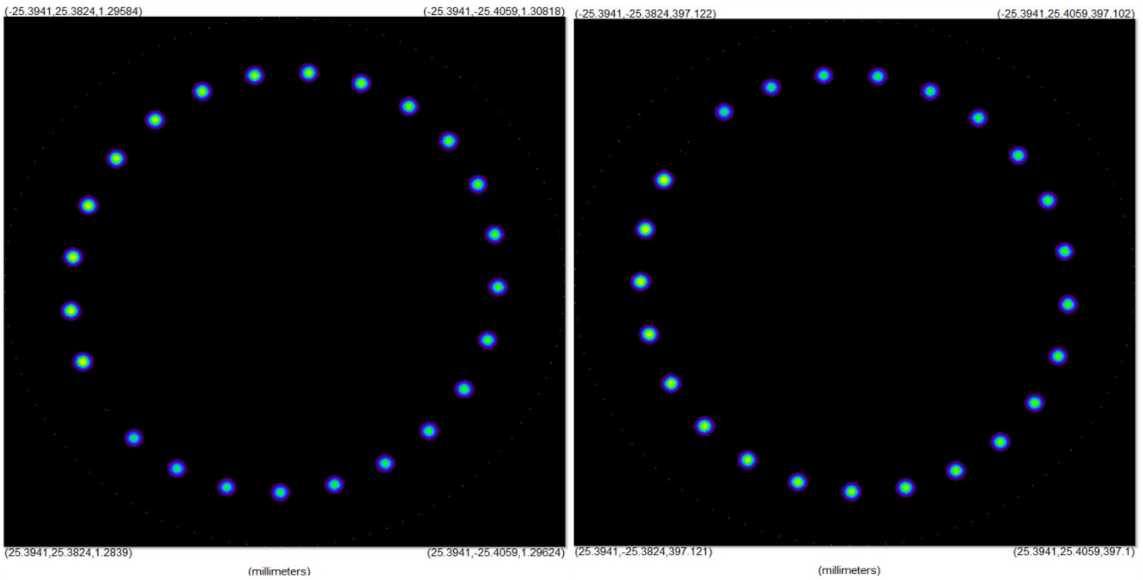

Fig. 14 Spot distribution diagram when $d = 398.3$ mm (the left side is spherical mirror A, the right side is spherical mirror B)

position. When the value of d is 193.9 mm, there are spots overlap, as shown in Fig. 12. The volume of the absorption cell is relatively large when the value of d is 398.4 mm, which is not conducive to miniaturization and sensitivity improvement. Therefore, $d = 206.5$ mm is the best choice, and it can be known from Tracepro software that the OPL is 19.8235 m. The error $|\Delta L|$ between the designed OPL and the simulated OPL is 3.5 mm, which is 0.017% of $L = 19.8200$ m.

Therefore, the given OPL can be achieved through multiple beam paths, but the parameters of the MPC can be selected and optimized according to actual needs. A Herriott-type MPC with the required OPL can be designed conveniently.

4 Conclusion

A variable OPL Herriott-type MPC design method is proposed in this paper. Simulation proves that it can achieve precise OPL with good continuity at a large range. The method is easy-to-implement, and it is expected to be applied to detect concentration in a large dynamic range and research the noise interference associated with MPC.

Acknowledgements This research is supported by the Major Program of the National Natural Science Foundation of China (Grant No. 61991430).

Compliance with ethical standards

Conflict of interest I would like to declare that this manuscript entitled "Design method of variable optical path length multi-pass cell" is original, has not been published before and is not currently being considered for publication elsewhere. We further confirm that the order of authors listed in the manuscript has been approved by all of us.

References

1. J.B. McManus, M.S. Zahniser, D.D. Nelson, Dual quantum cascade laser trace gas instrument with astigmatic Herriott cell at high pass number. Appl. Opt. **50**, A74–A85 (2011)
2. L. Shao, B. Fang, F. Zheng et al., Simultaneous detection of atmospheric CO and CH4 based on TDLAS using a single 2.3μm DFB laser. Spectrochim. Acta Part A: Mol. Biomol. Spectrosc. **222**, 117–118 (2019)
3. R. Cui, L. Dong, H. Wu et al., 3D-printed miniature fiber-coupled multi-pass cell with dense spot pattern for Ppb-level methane detection using a near-IR diode laser. Anal. Chem. **92**(19), 13034–13041 (2020)
4. W.R. Trutna, R.L. Byer, Multiple-pass Raman gain cell. Appl. Opt. **19**, 301–312 (1980)
5. G. Si, D. Yang, J. Guo et al., Optimization of Raman spectroscopy system for liquid detection in near concentric cavity and CO_3^{2-}/HCO_3^-detection. Spectrosc. Spectrosc. Anal. **39**, 1086–1091 (2019)
6. A. Sampaolo, G. Menduni, P. Patimisco et al., Quartz-enhanced photoacoustic spectroscopy for hydrocarbon trace gas detection and petroleum exploration. Fuel **277**, 118 (2020)
7. Y. Li, R. Wang, F.K. Tittel et al., Sensitive methane detection based on quartz-enhanced photoacoustic spectroscopy with a high-power diode laser and wavelet filtering. Opt. Lasers Eng. **132**, 106–155 (2020)
8. F. Xin, J. Guo, J. Li et al., Study on the measurement of CO_2 concentration by tunable semiconductor laser absorption spectroscopy. J. Ocean Univ. China **50**(08), 137–142 (2020)
9. F. Wu, C. Li, W. Shi et al., A spiral-shaped compact multi-optical path cell. Spectrosc. Spectral Anal. **36**(04), 1051–1055 (2016)
10. H. Xia, F. Dong, G. Tu et al., High-sensitivity detection of CO based on a new long optical path multiple reflection cell. Acta Opt. Sinica **30**(09), 2596–2601 (2010)
11. J.U. White, Long optical paths of large aperture. J. Opt. Soc. Am. **32**(5), 285–288 (1942)
12. D. Herriott, H. Kogelinik, R. Kompfner, Off-Axis paths in spherical mirror interferometers. Appl. Opt. **3**(4), 523–526 (1964)
13. Y. Cheng, X. Luo, L. Liu et al., Research on gas sensor with adjustable optical path. Sens. Microsyst. **35**(06), 56–58 (2016)
14. J.A. Silver, A.C. Stanton, Optical interference fringe reduction in laser absorption experiments. Appl. Opt. **27**, 1914–1916 (1988)
15. C. R. Webster, Brewster-plate spoiler: a novel method for reducing the amplitude of interference fringes that limit tunable-laser absorption sensitivities. Opt. Soc. Am. 1464–1470 (1985)
16. W. Liang, Q. Zhou, X. Dong et al., Influence of temperature-induced cavity length variation in wavelength modulation spectroscopy. Optik **172**, 220–224 (2018)
17. W. Liang, Y. Bi, Q. Zhou et al., Developing CH4 detection limit at $\lambda = 1.654\mu m$ by suppressing optical interference fringes in wavelength modulation spectroscopy. Sens. Actuators B Chem. **3**, 2614–2620 (2018)
18. J. Shemshad, S.M. Aminossadati, M.S. Kizil, A review of developments in near infrared methane detection based on tunable diode laser. Sens. Actuators B: Chem. **171**, 77–92 (2012)
19. D. Sakaizawa, C. Nagasawa, T. Nagai et al., Development of a 1.6 μm differential absorption lidar with a quasi-phase-matching optical parametric oscillator and photon-counting detector for the vertical CO_2 profile. Appl. Opt. **48**, 748–757 (2009)
20. J. Altmann, R. Baumgart, C. Weitkamp, Two-mirror multipass absorption cell. Appl. Opt. **20**(6), 995–999 (1981)
21. C.G. Tarsitano, C.R. Webster, Multilaser Herriott cell for planetary tunable laser spectrometers. Appl. Opt. **46**(28), 6923 (2007)
22. D. Mondelain, C. Camy-Peyret, A.W. Mantz et al., Performance of a Herriott cell, designed for variable temperatures between 296 and 20 K. J. Mol. Spectrosc. **241**(1), 18–25 (2007)
23. C.R. Webster, Measuring methane and its isotopes $^{12}CH_4$, $^{13}CH_4$, and CH_3D on the surface of Mars with in situ laser spectroscopy. Appl. Opt. **44**, 1226–1235 (2005)
24. J. Xu, X. Gong, F. Zhang et al., Design of NO_x gas measuring instrument based on nitrogen oxygen sensor. Sens. Microsyst. **34**(3), 90–93 (2015)
25. J. Xiang, Y. Chen, C. Xu et al., Research progress of surface acoustic NO_2 sensor sensitive film. Sens. Microsyst. **31**(9), 1–13 (2012)
26. J.B. McManus, P.L. Kebabian, M.S. Zahniser, Astigmatic mirror multpass absorption cells for long-path-length spectroscopy. Appl. Opt. **34**, 3336–3348 (1995)
27. J.B. McManus, P.L. Kebabian, Narrow optical interference fringes for certain setup conditions in multipass absorption cells of the Herriott type. Appl. Opt. **29**(7), 898–900 (1990)
28. D.R. Herriott, H.J. Schulte, Folded optical delay lines. Appl. Opt. **4**, 883–889 (1965)
29. R. Cui, L. Dong, H.P. Wu et al., Calculation model of dense spot pattern multi- pass cells based on a spherical mirror aberration. Opt. Lett. **44**(5), 1108 (2019)
30. R. Cui, L. Dong, H. Wu et al., Generalized optical design of two-spherical-mirror multi-pass cells with dense multi-circle spot patterns. Appl. Phys. Lett. **116**(9), 091103 (2020)
31. J. R. Pierce, Theory and design of electron beams. Van Nostrand, 194–197 (1954)